Journal of Materials Chemistry C

Accepted Manuscript

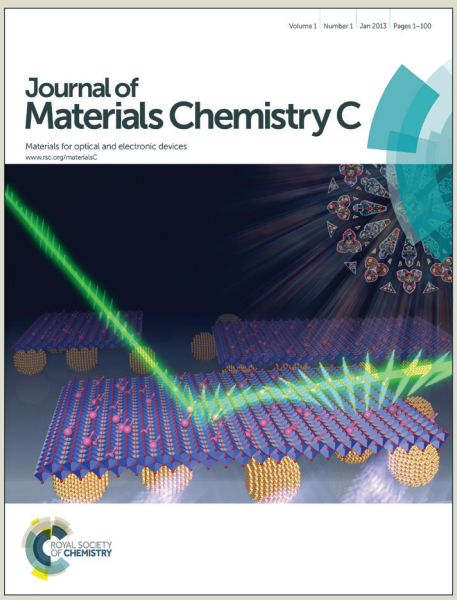

ROYAL SOCIETY OF CHEMISTRY

www.rsc.org/materialsC

Journal of Materials Chemistry C

Full PARER

Cite this: DOI: 10.1039/c0xx00000x

www.rsc.org/xxxxxx

Rare Earth-Free GaZnON Phosphor Prepared by Combustion for White Light-Emitting Diodes

Neelu Chouhan,[a][b]# Chun Che Lin,[a]# Shu-Fen Hu,*[c] and Ru-Shi Liu*[a][d]

# These authors contributed equally

Received (in XXX, XXX) Xth XXXXXXXXX 20XX, Accepted Xth XXXXXXXXX 20XX
DOI: 10.1039/b000000x

Nanophosphor GaZnON was synthesized by combustion using a unimolar mixture of metal oxides and urea as a flux/combustible agent at varying temperature and time, resulting products crystallized in a single monoclinic phase and had broad PLE spectra (300-550 nm at λ_{ex} = 350 nm) with the characteristic blue emission that can be utilised in white light-emitting diode by adding them with red and green light-emitting phosphors and by using UV LED (λ_{ex} = 300 nm). Phosphors were examined according to respective package parameters. The blue light-emitting phosphor GaZnON was found to have excellent potential in white light-emitting diode devices by assimilating them with already viable red and green light-emitting phosphors and by stimulating them using the near-UV LED chip with wavelength λ_{ex} = 300 nm. The possible electron transition mechanism responsible for the luminescence process was also discussed based on the experimental data.

1. Introduction

Photoelectronic devices such as ultraviolet light-emitting diodes (UV LEDs) have gained attention worldwide. These devices are used in long-term display systems (e.g., TV and computer or laptop screen), energy-saver solid-state lighting, solar cells, UV photolithography, high-density information storage, and biomedical sensors, among others. White light-emitting diodes (WLEDs) are also popular among illuminating devices because LEDs release only one particular color of light and produce extremely small amounts of heat, in contrast to white light produced by light bulbs or the sun. Semiconducting materials that belong to groups II to IV and III to V (i.e., ZnO, GaN- or doped GaN (InGaN)-based devices,[1] sulfide-based phosphors (e.g., SBP, such as SrS and CaS),[2] and p-type ZnO,[3] are generally used in WLEDs. Phosphors that are excited by GaN-based chips exhibit a pathetic color rendering index (CRI) at long wavelengths and limited visible light assessing ability. SBPs are degraded to volatile sulfur when SBPs are bombarded with high-energy electrons at low voltages; this condition pollutes emission tips and shortens life cycle of devices. Oxide phosphors have attracted considerable attention because they are used in light display systems (e.g., flat panel displays [FPDs] and field emission displays [FEDs]), vacuum fluorescent displays (e.g. VFDs), and enlightening systems. These oxide phosphors are widely used because oxide phosphors exhibit high-energy efficiency, superior chemical stability, photo-stability, excellent luminescent properties, durability, reliability, and products of various sizes and eco-friendly constituents.[4] However, a wide range of oxide phosphors, such as $CaSrSiO_4$,[5] Bi_2O_3/RuO_2,[6] $Ba_{0.93}Eu_{0.07}Al_2O_4$,[7] $Sr_{1-x}Ba_xSi_2O_2N_2:Eu^{2+}$,[8] $Y_3Al_5O_{12}:Ce^{3+}$,[9] $(Y,Tb)_3Al_5O_{12}:Ce^{3+}$,[10] $(Sr,Ba)_2SiO_4:Eu^{2+}$,[11] and $LiSrPO_4:Eu^{2+}$,[12] can be used in WLEDs. Most of the oxide phosphors contain either rare earth elements impurities/doping or phosphates. Phosphors with rare earth are expensive and phosphors with phosphates produce toxic fumes when heated (i.e., phosphine PH_3). But only few are recognised as rare earth element- and phosphate-free phosphors like BCNO,[13] AlBCON,[14] $K_2TiF_6:Mn^{4+}$,[15] $(Na_{1-x}Ca_x)(Sc_{1-x}Mg_x)Si_2O_6$,[16] $Ca_2NaZn_2V_3O_{12}$,[17] etc. Therefore, we synthesized an efficient phosphor without adding rare-earth elements or phosphates at comparatively mild reaction conditions. Furthermore, β-gallium oxide is considered as a thermal and chemical stable system compared with the rest of its polymorphs (i.e., α-, γ-, ε-, and δ-gallium oxide)[18] and inherent n-type nature because of slight oxygen deficiency. These oxygen vacancies act as a shallow donor with an ionization energy ranging from 0.03 eV to 0.04 eV;[19] these O vacancies promote the good properties in a phosphor. Doping usually improves photoluminescence quality of optoelectronic materials.

Hence, in this study, a binary compound GaZnON was synthesized through a low-cost combustion route that consisted of doping of a donor (Zn^{2+}) and acceptor (N^{3-}) to β-Ga_2O_3 with the

[a]Department of Chemistry, National Taiwan University No. 1, Sec. 4, Roosevelt Road, Taipei, 10617 Taiwan (R.O.C) E-mail: rsliu@ntu.edu.tw
[b]Department of Pure and Applied Chemistry, University of Kota, Kota, Rajasthan-324005 India
[c]Department of Physics, National Taiwan Normal University No. 88, Sec.4 Ting-Chou Rd., Taipei 116 Taiwan (R.O.C), E-mail: sfhu.hu@gmail.com
[d]Department of Mechanical Engineering and Graduate Institute of Manufacturing Technology, National Taipei University of Technology No. 1, Sec. 3, Zhongxiao E. Rd., Taipei, 10608 Taiwan (R.O.C.)

molecular formula $Ga_{2-x}Zn_xO_{3-x-y}N_y$, in which $x = 1$, $y = 1$. The GaZnON exhibited a monoclinic (space group = A2/m [12]) crystal structure that resembled to its parent semiconductor β-Ga_2O_3 (4.4 eV).[20–22] Furthermore, the luminescent properties of the blue light-emitting phosphor GaZnON (λ_{em} = 300 nm to 400 nm, band gap E_g = 3.3 eV) were investigated. Results suggested that the GaZnON can be used in optoelectronics and WLEDs; the use of this material can provide tough competition to the widely used gallium nitride WLEDs.[4]

2. Experimental

Well ground mixture of 0.94 g of zinc oxide (99%; Sigma–Aldrich), 1.08 g of β-gallium oxide (99.99%; Sigma–Aldrich), and 2 g of urea (97.98%; Sigma) in a silica crucible, was used to synthesize the gallium zinc oxynitride phosphor through combustion by varying the reaction temperature (200-900°C for 1h) and reaction time (1 to 7h at 300°C),[23] A shiny, voluminous, and off-white substance was obtained, as a reaction product because of the exothermic reaction that occurred between the mixture and the fuel. The exothermic reaction increased the system temperature up to > 1200°C. Finally, the highly sintered samples were soft milled to produce a powder. The powder was used as it is for the analysis.

3. Result and Discussion

The phosphor powder had the formula $Ga_{2-x}Zn_xO_{3-x-y}N_y$, in which $2 > x > 0$, $3 > y > 0$. In the experiment, urea was used as a flux and combustible fuel. Moreover, urea was added to enrich the lattice crystalline nature of the product and to lower the crystallization temperature. The TGA/DSC plot of the urea decomposition, which is shown in Fig. S1, shows the stepwise decomposition of the urea. Equations (1) to (4) show the most possible chemical reactions at the different DSC peaks.

At point A (161.3 °C, 72.5%, exothermic ⇒ experimentally 27.5% but theoretically 25% of urea consumed)

$(NH_2)_2CO_{(s)} \rightarrow NH_{3(g)} + HNCO_{(l)}$ .....(1)

At point B (277.3 °C, 65%, exothermic ⇒ experimentally 35% but theoretically 36% of urea consumed)

$HNCO_{(l)} + H_2O_{(l)} \rightarrow NH_{3(g)} + CO_{2(g)}$ .....(2)

At point C (554.8 °C, 55%, exothermic ⇒ experimentally and theoretically 45% of urea consumed)

$2NH_{3(g)} \rightarrow N_2H_{4(g)} + H_{2(g)}$ .....(3)

At point D (745.8 °C, 50%, exothermic ⇒ experimentally and theoretically 50% of urea consumed)

$N_2H_{4(g)} \rightarrow 2H_{2(g)} + N_{2(g)}$.....(4)

NH_3 released from urea at high temperature helps to introduce nitrogen and Zn from ZnO to the gallium oxide lattice. NH_3 was produced during the reaction 1 and 2, started to decompose to N_2H_4 and hydrogen, as evident from the TGA/DSC reactions shown in Equations (1) to (3). Eventually at point D, the thermal decomposition of hydrazine produced N_2 and H_2 at 745.8°C (actually this temerature will raise up to 1200°C). N_2H_4 and H_2, both are jointly responsible for the reductive atmosphere.[24] This behavior promoted gradual phase transition, which was also supported by the XRD results. Therefore, representative synthesis at 300°C for 1 h was performed. The reductive atmosphere induced the reduction of ZnO and Ga_2O_3 species during the nitridation process; however, excess Zn was not observed, which was also confirmed by the XRD, energy-dispersive X-ray spectroscopy (EDX), and XAS results. The results showed that reduced Zn inserted into the Ga_2O_3 lattice.

XRD and Morphological aspects

Fig. 1a shows the crystal structure and XRD patterns of the phosphor GaZnON, which was prepared at temperatures ranging from 200°C to 900°C for 1 h. Figs. 1b and 1c display the $Ga_{2-x}Zn_xO_{3-x-y}N_y$ (x = 1 and y = 1) samples annealed between 1 to 7 h at 300°C and the standard β-Ga_2O_3 (JCPDS card no. 11-370), respectively. The diffraction patterns of all the synthesized samples at temperatures ranging from 200°C to 400°C for 1 h closely resemble to the reference data of the host β-Ga_2O_3. The aforementioned systems crystallized in a single phase, which indicates that the ZnO (MP = 1975°C) successfully dissolved in the host lattices β-Ga_2O_3 (MP = 1750°C) during combustion. This process augmented the acceptor–donor pair Zn^{2+} and N^{3-} to the host. GaZnON crystallized in a monoclinic phase, owning a space group *A2/m* [12], Pearson symbol *mC20*, where four GaZnON formula units are present in a unit cell (Z = 4). The calculated lattice parameters included a = 5.80 nm, b = 3.04 nm, c = 12.23 nm, β = 103.6°, and volume = 209.5 Å^3; these results were consistent with reported data.[25] Increase in the reaction temperature caused phase distortion in the sample prepared between 500 and 900°C. Similarly, the XRD patterns (Fig. 1b) of the seven compounds produced at 300°C and between 1 to 7 h show a single and stable monoclinic phase. The crystalline size (6.98 nm) of the phosphor was estimated using Debye-Scherrer equation on three strong peaks (200), (111) and (110) of the GaZnON sample for the GaZnON sample synthesized at 300°C for 1 h.

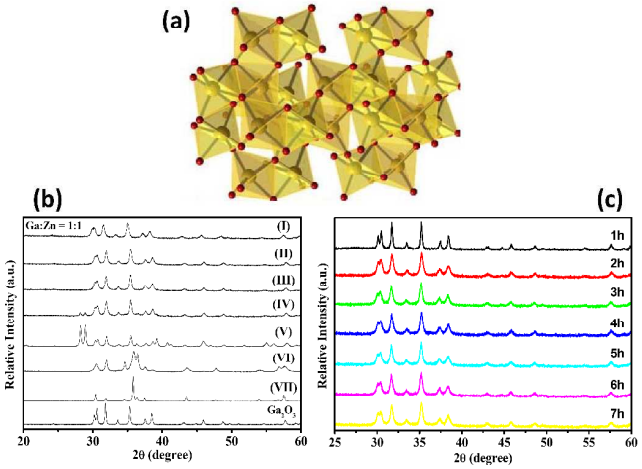

Figure 1. (a) Monoclinic crystal structure of GaZnON and XRD patterns of solid solution GaZnON at (b) varying synthesis temperatures of (I) 200, (II) 300, (III) 400, (IV) 500, (V) 600, (VI) 700, and (VII) 900°C and pure β-Ga_2O_3 synthesized at (c) 300°C for 1 h to 7 h.

The particle size, which was estimated using XRD, was consistent with the results obtained from the morphological overview obtained through FESEM/HRTEM (Figs. 2a and 2c). The 1D crystalline nature of the product was computed using the Segal empirical formula Eq. (5).[26]

$C_{rf}\% = \{(I_{002}-I_{am})/I_{002}\} * 100$.....(5)

Where, C_{rf}% = the relative crystallinity (in percentage); I_{002} = the highest intensity of the (002) diffraction angle of the crystal lattice (arbitrary unit; au); and I_{am} = the scattering strength diffracted by the non-crystalline environment (if 2θ is close to 21°, the unit is similar with I_{002}). In this particular case, the respective values of I_{002} and I_{am} were 1897.2 and 623.84 au.

Hence, the studied sample possessed 67.10% relative crystallinity, which was close to the values observed by FESEM and HRTEM. Spherical shaped particles, with sizes ranging from 6.5 to 13.0 nm, were observed from the FESEM images (Fig. 2a).

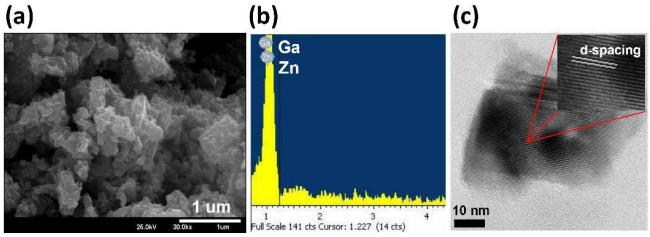

Figure 2. (a) FESEM image of sample synthesized at 300°C and 1 h, (b) corresponding EDX profile of sample and (c) HRTEM image showing lattice fringes separated by a distance of 0.61 nm. This result indicates that the crystal growth direction was along the reflection planes (111) and (002).

Sometimes, edges are not clearly defined in FESEM images; thus, difference observed between the results obtained from the Scherrer equation and FESEM images. The corresponding EDX profile of the both series of GaZnON prepared at different temperatures and time periods were used to estimate the metallic composition of the products, which are shown in Tables S1 and S2. The concentrations of N and O in the sample were not measured accurately by EDS. Thus, the XAS at N and O K-edge study was used to determine the O and N presence/effect. The overlapped Zn and Ga EDX signals (Fig. 2b) indicates the roughness of the synthesized powder sample. Meanwhile, the Ga/Zn ratios for both respective series were almost similar (1.0–1.4) and (0.72–1.4), as shown in the corresponding Tables S1 and S2.

Although both oxides were present in equal amounts (ZnO; β-Ga_2O_3 = 1:1) at the beginning of the reaction, a low concentration of Zn compared with gallium was observed at the end of the reaction because of the volatile nature of Zn. The HRTEM (Fig. 2c) was used to verify the crystalline nature of the GaZnON. Uniform lattice fringes were ordered at inter-plane d-spacing of 0.61 nm (Table S3), corresponds to the reflection planes (111) and (002). That reconfirms the highly crystalline nature of the sample and exhibits the crystal growth direction i.e, along 111 and 002 planes. The observed d-spacing is competent enough to match with the parent compound β-Ga_2O_3 crystal (JCPDS card no. 11-370).

Band Structure and Mechanism of Electron Transition

Figs. 3a and 3b display the characteristic diffuse reflectance spectrum of the samples synthesized under different time (1 h to 7 h) periods and at constant reaction temperature (i.e., 300°C) and band diagrams at different stages of the gradual modification of the host β-Ga_2O_3, respectively. No specific changes in the sample produced at 200°C for 1 h with respect to the pristine β-Ga_2O_3 were exhibited. Therefore, the samples crystallized in a pure phase at 300°C for 1 h was used in subsequent analyses (e.g., DRS and XAS). A steady increase in the onset wavelength or decrease in the corresponding band gap, which was calculated using Kubelka–Munk function F(R) vs λ plots, as shown in Table S2, was observed for the systems prepared at different time (1 h to 7 h) periods. The samples heated for 1, 2 and 3 h demonstrated single-hump parabolic curves with their respective band gaps, viz. 3.53, 3.48, and 3.22 eV. Furthermore, the samples heated at 4, 5, 6, and 7 h showed double-hump curves with almost constant band gaps of 3.21, 3.21, 3.23, and 3.20 eV, respectively. The above measurements confirmed the reduction in the band gap of the β-Ga_2O_3 (4.40 eV), which was attributed to the insertion of the elements (i.e., Zn and N) into the β-Ga_2O_3 lattice. A prominent repulsion between the 3d electrons of Zn and 2p electrons of O and N in the valance band (VB) of the GaZnON expanded the VB; consequently, the upper edge of the VB moved up. Similarly, the repulsion between the electrons of the Zn (4s) and Ga (4s4p) orbitals in the conduction band (CB) expanded the CB. Augmentation of both phenomena resulted in reduction of the band gap of the phosphor, as shown in Fig. 3b. Furthermore, decreased band gap of the GaZnON increased the DRS peak heights along with the red shift in the onset wavelength, which confirmed the formation of the solid solution.

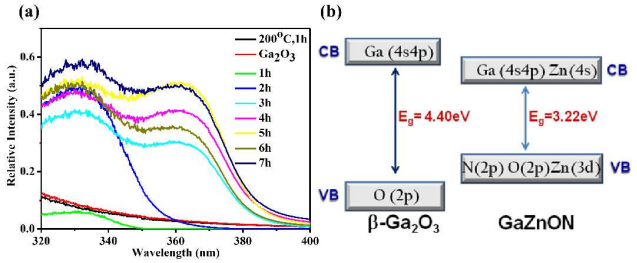

Figure 3. (a) DRS profile of solid solution prepared at 300 °C and different time (1 h to 7 h) periods and (b) comparative changes in band edge positions of pristine β-Ga_2O_3 when Zn and N species are added.

X-ray absorption near-edge structure (XANES) studies at O and N *K*-edge

In *K*-edge XAS, a *K* electron moves to an unoccupied state of a photoexcited system when an x-ray photon is absorbed by the electron. Afterwards, the transitions of the photoelectron to either bound or free state is subject to the dipole selection rules. This behavior can be used as a useful parameter to investigate the unoccupied atomic or molecular orbitals or local geometry around the monitoring species. Waves of the circulating spherical photoelectron scattered (multiple/single) by vicinity atoms result in interference intercalate changes in the surrounding areas of an absorbing atom; thus, fluctuations in the absorption cross section are observed in the XAS profile of the sample. Here, O and N *K*-edge XANES studies are used to examine the local atomic surroundings/sites around the O and N atoms, respectively, in the solid solution GaZnON. Fig. 4a illustrates the normalized O *K*-edge absorption spectrum, which was attributed to the O 1s electron that was excited to an unoccupied O 2p state and resulted in a photoelectron that hybridized with different metallic atomic orbitals. The photon energies are assigned to the following hybridized states in the XANES spectra.

Pre-edge peak (529 eV) → O 2p hybridized with Zn 3d/Ga 3d
White line maxima(539 eV) → O 2p hybridized with Zn 4s/Ga 4s
XANES peaks(539-550eV) → O 2p hybridized with Zn 4p/Ga 4p
EXAF peaks (> 550 eV) → O 2p hybridized with Zn 4d/Ga 4d

All of the GaZnON samples exhibited similar XANES patterns but different intensity with respect to the β-Ga_2O_3. This finding suggests that all atomic species belong to the same crystal system of different isotropic nature. The pre-edge features, attributed to the O (2p) vacancies, which were caused by the replacement of two O in Ga_2O_3 by one N atom in GaZnON.[27] Hieght of the pre-edge peak was proportional to the O (2p) vacancies increased with nitridation time (1 h to 6 h) at a reaction temperature of 300°C. However, the sample heated for 7 h exhibited

comparatively weak peaks because of decrease in void size or number of voids. Heating caused evaporation of metallic species Zn/Ga and O_2 from GaZnON lattice and insertion of one Zn and one N at the cost of one Ga and two O, respectively.

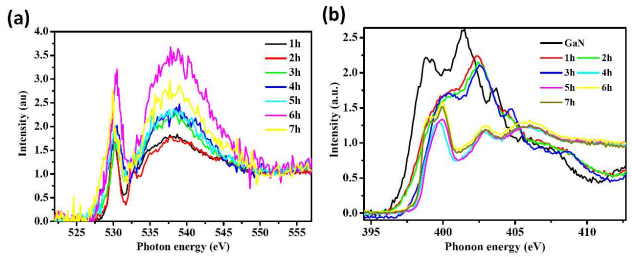

Figure 4. XAS profiles of GaZnON samples synthesized at 300 °C from 1 h to 7 h: (a) O *K*-edge and (b) N *K*-edge.

This phenomenon caused voids/oxygen deficiency that justified by the spin-split impurity band model of Coey et al.[28-29] According to which asymmetry was facilitated by the inter-site coulomb interaction and local coordination. These phenomena multiplied by the existence of Zn 3d (E~ −10 eV) atoms at the shallow level in compare to Ga 3d level (E~ −20 eV).[30] Unlike the Ga 3d level, the Zn 3d level was not completely localized at the deep core level. Therefore, the Zn 3d orbitals powerfully hybridized with the O 2p orbital and the unoccupied Zn 4sp bands; this condition generated localized holes in the shallow VB.[31] These localized holes magnified the columbic interaction and induced efficiency through atomic reshuffling.[32] On the contrary, the deeply situated Ga 3d level did not generate localized holes; thus, the Ga 3d level did not contribute large to active sites. For this reason, in spite of GaO_5 distortion in ZnO_5 cluster was observed. Hence, the localized Zn hole may act as a hopping hub,[31,32] which allows Ga 4s electrons to hop and contribute significantly in electrical conduction. Strong transition between the photoelectron and non-bonding electrons caused elevation in the broad white line peaks when reaction time increased from 1 h to 6 h of thermal exposure. Moreover, a short white line peak was observed at the phonon energy 537 eV after 7 h of thermal exposure because of low degree of p-band defects. The thermal vibrations and static disorder in the lattice caused high anisotropic arrangement of the elements around the O atom. The EXAFS features of all the studied samples included a shoulder peak at PE = 561 eV, followed by an extraordinarily long and broad third and fourth peaks at PE = 573 and 584 eV, respectively. These significant features show that the anions surrounded the central Zn atoms in a distorted tetrahedral/octahedral fashion; this behavior altered the lattice parameters of the product with respect to the parent compound.[33]

The N *K*-edge measurements on the solid solutions of the GaZnON (synthesized at 1 h to 7 h) and the standard GaN were used to plot the typical normalized X-ray absorption cross section against PE, as demonstrated in Fig. 4b. The spectrum of the crystalline material was consistent with the data available in literature.[34–36] The experimental XANES profiles and edges of the XAS profiles of the all studied solid solutions with respect to GaN shifted toward high PE when reaction time was increased. The finding implies that the substitution of N by O increased with increased reaction time. The study was divided into two classes according to XANES profile patterns: the first class involved the standard GaN and samples heated from 1 h to 3 h and the second class included the samples heated for 4 h to 7 h at 300°C. The first class showed weak XANES feature with photon energy at 399.0 eV that corresponds to the transition between the *K*-shell electron of the N(1s) to the unoccupied p_z (out-of-plane; p-band) electron (1s–π* resonance, π bond), which is assigned to the metal–nitrogen (M–N) bond.[37] At PE = 402.5 eV, a strong non-excitonic signals appeared along the minor shift of 0.50 eV at the high energy side, which were attributed to the characteristic π* transition (i.e., N(1s) → unoccupied 2p)[38] that confirmed the remarkable presence of a interstitial molecular N_2.[39] A relatively broad and short peak around 405 eV, which is a result of the σ* transition between the N(1s) → unoccupied p_{xy} and where the M–N bonds lie in the bilayer position (in-plane, σ-bond), was observed.[40] The presence of the above two peaks were attributed to the sp^2 (1s → π*) and sp^3 (1s → σ*), respectively, which dominated the environments of the transition metal nitrides.[41,42] This finding implies the presence of one strong out-of-plane and three weak in-plane bonding of the crystal structure. The second class exhibited reverse results with respect to the previous class. The height of the WL peak increased and decreased in the non-excitonic peak (PE = ~402.5 eV) height, and a red shift in PE was observed. This finding showed the increased number of unoccupied metallic states (4s and 4d) in the CB; however, the systems retained a similar crystal system for GaZnON.[43] A strong absorption for the transition of electron from N 1s to the unoccupied p_{xy} states was observed. This finding reflected the σ-bond nature and the sp^3 arrangement of the metallic species around N_2. Similarly, the strong absorption peak around 407 eV,[44] which was dominated by the N 1s → unoccupied p_z transition and corresponded to the π-bond character, revealed the presence of three strong in-plane M–N bonds (σ bond) and one weak out-of-plane M–N (π bond) bond in the crystal structure. The results suggested a tetrahedral arrangement of the GaZnON system, where the metallic species Zn and Ga are at the center of the tetrahedra and both anions (i.e., N^{3-} and O^{2-}) situated at the four apices of the teterahedra.

The comparative excitation and broad emission spectrum of the pristine β-Ga_2O_3 and GaZnON samples synthesized at 200, 300, 400, and 500°C, are demonstrated by the Figs. 5a and 5b, respectively, which depended on structural and temperature conditions.[45-47] Under the emission radiation λ_{em} = 392 nm, the excitation peaks of the samples were λ_{ex} = 380, 424, 426, 405, and 401 nm, as shown in Fig. 5a. The excitation spectra consist of two principal excitation bands; first, at the middle UV range (200-300 nm) and second, at the near UV range (300-426 nm). The first peak was attributed to the transition of the host electron between the VB and CB.[48] The second peak was correlated to the direct excitation of the host electrons to the dopant (Zn and N). The representative broad emission spectrum with emission maxima (at λ_{ex} = 300 nm, λ_{em} = 426, 386, 394, 402, 410, 415 nm) and their corresponding full width at half maximum (FWHM) 113, 139,140, 20, and 11 nm, are illustrated in Fig. 5b.

The photoluminescence emission (PLE) is a result of the relaxation of an excited-state electron from their excited state to a completely relaxed ground level, responsible for zero-phonon lines and signified the right side of the emission spectrum. Simultaneously, the coupling of the longitudinal optical phonons with the host lattice vibrational modes results the left side of the PLE spectrum. The GaZnON samples synthesized at 300 °C and 1 h to 7 h demonstrated excitation peaks under λ_{em} = 392 nm and at λ_{ex} = 348, 353, 336, 335, 329, 336, and 336 nm (Fig. 6a). The emission crests for the same series was recorded under the excitation wavelength λ_{ex} = 350 nm, are reported at λ_{em} = 380, 391, 400, 400, 403, 397 and 404 nm (Fig. 6b) along with their respective FWHM i.e., 6.3, 8.3, 6.6, 5.9, 4.5, 5.6, and 5.0 μm (Table S4). Figs. 7a, 7b, and 7c along with the Tables S4 and S5 displayed the Commission International de l' Eclairage (CIE) and

chromaticity coordinates of both classes of the GaZnON, respectively. The Quantum efficiency of GaZnON phosphors with different reaction temperature were described in Table S6.

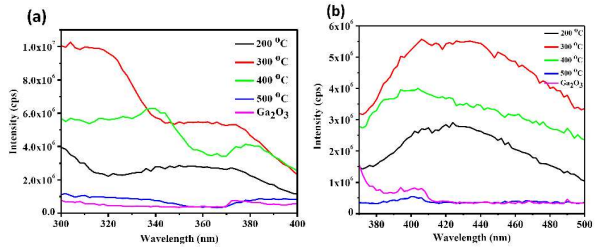

Figure 5. (a) Excitation (λ_{em} = 392 nm, λ_{ex} = 424, 426, 405, 401, and 380 nm) and (b) emission spectra (λ_{ex} = 300 nm, λ_{em} = 386, 394, 402, 410-415, and 426 nm) of GaZnON synthesized at 200, 300, 400, 500 °C and pristine β-Ga_2O_3.

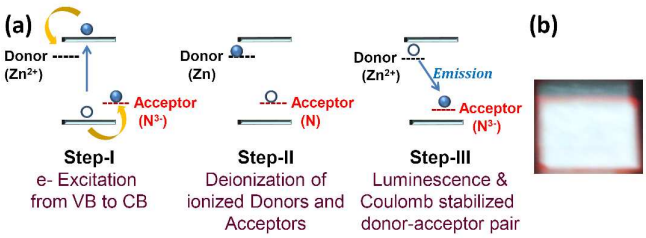

Scheme 1. (a) Donor–acceptor pair luminescence mechanism and (b) Blue phosphor $Ga_{2-x}Zn_xO_{3-y}N_y$ (x = 1 and y = 1) synthesized at 500 °C and 1 h and exposed to UV light.

The partly filled d-orbital of the Ga and Zn ions (d–d transitions) originated the broad-band emission peak in the GaZnON. The observed extremely broad emission spectra were attributed to the two basic mechanisms i.e., either through charge transfer luminescence[49] or donor–acceptor pair luminescence or both.[50] Charge transfer optical transition usually occurs between different kinds of metal orbitals of similar ion/atom or electronic states of different ions. Such transition promoted strong changes in the charge distribution around the optical center. This result caused significant changes in chemical bonding. It was observed the bonding environment of the samples heated for 1 h to 3 h at 300°C remains almost unchanged and on the other hand changes in bonding observed for the samples heated for 4 h to 7 h at 300°C. The luminescence follow the donor–acceptor pair luminescence mechanism when semiconducting materials (β-Ga_2O_3) are doped with both donors and acceptors (i.e., Zn^{2+} and N^{3-}, respectively), as illustrated in Scheme 1. The broad emission bands in the blue-light emitting phosphor material originated from a strong electron–phonon coupling between the electronic defect and the vibaronic lattice states. The energy separation among the emission of each of the individual donor–acceptor pairs decreased because of the large donor–acceptor distance (low energies). This condition caused formation of a broad emission band, which was associated with the red shift.

The WLED devices were manufactured by combining commercially available red, green, and blue light-emitting phosphors that were excited by near UV LED chip ($\lambda_{ex} \approx$ 300 nm). Here the GaZnON can be used as the blue-emitting component of WLED. Both categories of the synthesized phosphors exhibited outstanding CIE chromaticity coordinates, as demonstrated in Figs. 7a, 7b, and 7c and Tables S4 and S5. The CIE coordinates showed that although variation in the synthesis temperature was used, the GaZnON still exhibited the same blue light emission. However, variation in the synthesis time showed interesting results. The sample synthesized at 1, 5, 6, and 7 h emitted blue light, and the samples heated for 2, 3, and 4 h ignites emitted red light. Moreover, the package parameters presented in the Table S5, involved the phosphor weight (%), luminance L_v (milicandela), CIE-x, CIE-y, luminous intensity I_v (lumen), power W (mW), and luminous efficiency V_f (V). These properties were determined for the GaZnON synthesized at the different temperatures, and the results confirmed the excellent properties of the GaZnON compared with those of the β-Ga_2O_3, for WLEDs. All of the studied samples showed high luminous efficiency (3.28, 3.28, 3.34, and 3.47 V) at low power consumption (0.88, 0.54, 1.79, and 1.91 mW) with respect to the β-Ga_2O_3 (3.17 V at 3.36 mW). The package data, good thermal and structural stability of the host, and excellent CIE coordinates are properties that enable GaZnON as a promising blue light component of LEDs, which can be widely used in the white LED industries.[51]

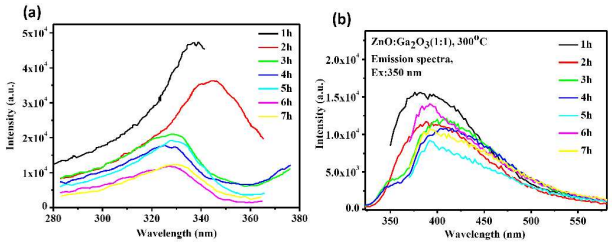

Figure 6. (a) Excitation (λ_{em} = 392 nm, λ_{ex} = 348, 353, 336, 335, 329, 336, and 336 nm) and (b) emission spectra (λ_{ex} = 350 nm, λ_{em} = 380, 391, 400, 400, 403, 397, and 404 nm) of the phosphor GaZnON ignited for 1 h to 7 h.

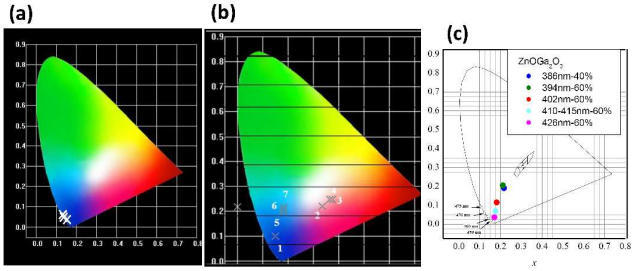

Figure 7. CIE coordinates of (a) GaZnON synthesized at 200, 300, 400, and 500°C and pristine β-Ga_2O_3 sample, (b) GaZnON synthesized at 300°C and calcined at 1 h to 7 h and (c) package parameters.

4. Conclusions

GaZnON solid solution was successfully synthesized through the combustion of the unimolecular mixture of the zinc oxide and gallium oxide in presence of the urea by varying temperatures and reaction times. Urea behaved as a fuel to increase the reaction temperature up to 1200°C and also as a flux to improve the crystallinity of the solid solution. XRD and SEM/EDS results showed that the product $Ga_{2-x}Zn_xO_{3-y}N_y$ (x = 1 and y = 1) crystallized in a pure monoclinic phase, and spherical particles ranging from 6 nm to 13 nm grew along the (002) and (111) planes. HRTEM and SAED images of the compound confirmed the presence of uniform and ordered lattice fringes. DRS measurements provided evidence that the elements (i.e., Zn and N) inserted into the β-Ga_2O_3 (E_g = 4.40 eV) lattice, which decreased the band gap of the solid solution from 3.53 eV to 3.21 eV. XAS results revealed the local atomic arrangement around O and N and further verified the presence of the M = N bond and O

deficiency in the compound, where the centrally occupied Ga/Zn was tetrahedrally surrounded by O/N at apexes position. GaZnON exhibited blue luminescence with different broadband (300 nm to 550 nm) emission peaks at λ_{ex} = 300 nm and ultraviolet excitation at 350 nm. These emission peaks are λ_{em} = 386, 394, 402, 410, and 415 nm for samples synthesized at 200–500°C for 1 h, and λ_{em} = 380, 391, 400, 400, 403, 397, and 404 nm for the compound formed at 300°C for 1–7 h, respectively. The mechanisms of electron transition of the solid solution may involve donor–acceptor pair or charge-transfer luminescence. Results of PLE and information obtained from the package data confirmed that the compound was a good phosphor for WLEDs.

5. Acknowledgements

The authors thank the Ministry of Science and Technology, Taiwan (Contract Nos. MOST 101-2113-M-002-014-MY3 and 103-2112-M-003-009-MY3) and the Science and Engineering Research Board of the Department of Science and Technology, India (SB/S1/PC-31/2012) for their financial support. We also acknowledge the National Synchrotron Radiation Research Centre, Taiwan for allowing us to use the beam line (BL20A) to study the samples at the O and N *K*-edges.

6. Notes and Reference

[1] E. J. Shin, N. W. Song, J. I. Lee and D. Kim, *J. Kor. Phys. Soc.* 1998, **33**, S295.
[2] V. Singh, M. Tiwari and S. J. Dhoble, *Ind. J. Pure Appl. Phys,.* 2005, **43**, 100.
[3] B. Xiang, P. Wang, X. Zhang, S. A. Dayeh, D. P. R. Aplin, C. Soci, D. Yu and D. Wang, *Nanoletters,* 2007, **7(2)**, 323.
[4] (a) S. Nakamura, T. Mukai and M. Senoh, *Appl. Phys. Lett.,* 1994, **64,** 1687. (b) T. Nishida, T. Ban and N. Kobayashi, *Appl. Phys. Lett.,* 2003, **82**, 3817. (c) E. F. Schubert, J. K. Kim, *Science* 2005, **308(5726),** 12741278. (d) T. Hashimoto, F. Wu, J. S. Speck and S. Nakamura, *Nat. Mater.,* 2007, **6**, 568.
[5] S. Tezuka, Y. Sato, T. Komukai, Y. Takatsuka, H. Kato and M. Kakihana, *Appl. Phys. Express,* 2013, **6 (7)**, 72101.
[6] Y.-C. Chu, G.-J. Lee, C.-Y. Chen, S.-H. Ma, J. J. Wu, T.-L. Horng, K. H. Chen and J.-H. Chen, *J. Nanomaterials* 2013, **2013**, 596324.
[7] X. Li, J. D. Budai, F. Liu, J. Y. Howe, J. Zhang, X.-J. Wang, Z. Gu, C. Sun, R. S. Meltzer and Z. Pan, *Light: Science & Applications,* 2013, **2**, e50.
[8] I. H. Cho, G. Anoop, D. W. Suh, S. J. Lee and J. S. Yoo, *Optical Materials Express,* 2012, **2 (9),** 1292.
[9] A. A. Setlur, *The Electrochemical Society* : *Interface*. Winter 2009, 32.
[10] J. K. Park, M. A. Lim, C. H. Kim, H. D. Park, J. T. Park and S. Y. Choi, *Appl. Phys. Lett.,* 2003, **82**, 683.
[11] J. K. Park, K. J. Choi, S. H. Park, C. H. Kim and H. K. Kim, *J. Electrochem. Soc,.* 1968, **115**, 642.
[12] C. C. Lin, Z. R. Xiao, G.-Y. Guo, T.-S. Chan and R.-S. Liu, *J. Am. Chem. Soc.*, 2010, **132 (9)**, 3020.
[13] W-N Wang, T. Ogi, Y. Kaihatsu, F. Iskandar and K. Okuyama *J. Mater. Chem.*, 2011, **21**, 5183.
[14] T. Ogi, H. Iwasaki, A. B. D. Nandiyanto, F. Iskandar, W.-N. Wang and K. Okuyama *J. Mater. Chem. C*, 2014, **2**, 4297
[15] H. Zhu, C. C. Lin,W. Luo, S. Shu, Z. Liu, Y. Liu, J. Kong, E. Ma, Y. Cao, R-S. Liu, and X. Chen, *Nature Commu*., 2014, **5**,4312.
[16] Z. Xia, Y. Zhang, M. S. Molokeev, V. V. Atuchin, Y. Luo, *Scientific Report*, 2013, **3**, 3310.
[17] C. Xue, X. Zhiguo, Y. Min, W. Xiachan, X. Hao, *J. Phys. and Chem Solids*, 2013, **74**, 1439.
[18] R. Roy, V.G. Hill and E.F. Osborn, *J. Am. Chem. Soc.,* 1952, **74**, 719.
[19] M. Ogita, N. Saika, Y. Nakanishi and Y. Hatanaka, *Appl. Surf. Sci*., 1999, **142**, 188.
[20] H. H. Tippins, *Phys. Rev*., 1965, **140,** A316.
[21] Z. Hajnal, J. Miró, G. Kiss, F. Réti, P. Deák, R.C. Herndon and J.M. Kuperberg, *J. Appl. Phys*., 1999, **86,** 3792.
[22] H.-G. Kim and W.-T. Kim, *J. Appl. Phys*., 1987, **62**, 2000.
[23] J. J. Kingsley and K. C. Patil, *Mater. Lett.*, 1988, **6**, 427.
[24] D. Dirtu, L. Odochain, A. Pui and L. Humelnicu, *Central European J Chem.*, 2006, **4(4),** 666.
[25] J. A. Kohn, G. Katz and J. D. Broder, *American Mineral*, 1957, **42(5-6)**, 398.
[26] L. Segal, J. J. Creely and A. E. Martin, *J. Textile Research,* 1959, **29**, 786.
[27] J. J. Rehr, R. C. Albers and S. I. Zabinsky, *Phys. Rev. Lett.,*1992, **69(23),** 3397.
[28] J. M. D. Coey, M. Venkatesan and C. B. Fitzgerald, *Nat. Mater.,* 2005, **4**, 173.
[29] D.-Y. Cho, J. Song, K. D. Na, C. S. Hwang, J. H. Jeong, J. K. Jeong and Y.-G. Mo, *Applied Physics Letters,* 2009, **94**, 112112.
[30] J.-H. Guo, L. Vayssieres, C. Persson, R. Ahuja, B. Johansson and J. Nordgren, *J. Phys.: Condens. Matter,* 2002, **14**, 6969.
[31] S.-H. Wei and A. Zunger, *Phys. Rev. B,* 1988, **37**, 8958.
[32] C. L. Dong, C. Persson, L. Vayssieres, A. Augustsson, T. Schmitt, M. Mattesini, R. Ahuja, C. L. Chang and J.-H. Guo, *Phys. Rev. B,* 2004, **70**, 195325.
[33] E. A. Stern, "Theory of EXAFS" in X-ray absorption: Principles, Applications, Techniques of EXAFS, SEXAFS and XANES, (Eds: D. C. Koningsberger, R. Prins) *Wiley-Interscience,* New York, 1988, ***Ch.8*** pp 618-708.
[34] Y. L. Soo, S. Huang, Y. H. Kao, J. G. Chen, S. L. Hulbert, J. F. Geisz, S. Kurtz, J. M. Olsen, S. R. Kurtz, E. D. Jones and A. A. Allerman, *Phys. Rev. B,* 1999, **60**, 136105.
[35] W. R. L. Lambrecht, S.N. Rashkeev, B. Segall, K. Lawnicak-Jablonski, T. Suski, E.M. Gullikson, J. H. Underwood, R. C. C. Perera, J. C. Rife, I. Grzegory, S. Porowski and D. K. Wickenden, *Phys. Rev. B,* 1997, **55**, 2612.
[36] K. Lawnicak-Jablonski, T. Suski, I. Gorczyca, N.E. Christensen, K.E. Attenkofer, R.C.C. Perera, E.M. Gullikson, J.H. Underwood, D.L. Ederer and W. Z. Liliental, *Phys. Rev. B,* 2000, **61**, 16623.
[37] M. Terauchi, *Microsc. Res. Tech*., 2006, **69,** 531.
[38] S. C. Ray, H. M. Tsai, C. W. Bao, J. W. Chiou, J. C. Jan, K. P. K. Kumar, W. F. Pong, M.-H. Tsai, S. Chattopadhyay, L. C. Chen, S. C. Chien, M. T. Lee, S. T. Lin andK. H. Chen, *J. Appl. Phys.*, 2004, **96(1)**, 208.
[39] J. B. Metson, H. J. Trodahl, B. J. Ruck, U. D. Lanke and A. Bittar, *Surf. Interface Anal.* 2003, **35**, 719.
[40] I. Jimenez, W. M. Tong, D. K. Shuh and F. Himpsel, *Appl. Phys. Lett*., 1996, **68(20)**, 2816.
[41] L. J. Terminello, A. Chaiken, D. A. Lapiano-Smith, G. L. Doll and T. Sato, *J. Vac. Sci. Technol. A,* 1994, **12**, 2462.
[42] R. Kapoor, S. T. Oyama, B. Fruhgerger and J. G. Chen, *Catal. Lett.,* 1995, **34**, 179.
[43] H. Chen, W. Wen, Q. Wang, J. C. Hanson, E. Muckerman, A. Fujita, I. Frenkel, and J. A. Rodriguez, *J. Phys. Chem. C*, 2009, **113**, 3650.
[44] (a) L. Li, M. Proti`ere, M. Re and P. Reiss, *Chem. Mater.*, 2008, **20**, 2621 (b) K. L. Jablonska, T. Suski, I. Gorczyca, N. E. Christensen, K. E. Attenkofer, R. C. C. Perera, E. M. Gullikson, J. H. Underwood, D. L. Ederer and Z. L. Weber, *Phys. Rev. B: Condens. Matter Mater. Phys*., 2000, **61**, 16623.
[45] A. Van Dijken, E. A. Meulenkamp, D. Vanmaeklenbergh and A. Meijerink, *J. Lumin.,* 2000, **87-89**, 454.
[46] Y. J. Xing, Z. H. Xi, Z. Q. Xue, X. D. Zhang, J. H. Song, R. M. Wang, J. Xu, Y. Song, S. L. Zhang,and D. P. Yu, *Appl. Phys. Lett.,* 2003, **83,** 1689.
[47] D. C. Oh, T. Suzuki, J. J. Kim, H. Makino, T. Hanada, M. W. Cho and T. Yao, *Appl. Phys. Lett.,* 2005, **86**, 032909.
[48] C.W. Yeh, Y.P. Liu, Z. R. Xiao, Y. K. Wang, S. F. Hu and R. S. Liu, *J. Materials Chem. A,* 2012, **22,** 5828.
[49] (a) E. Nakazawa, *Chem. Phys. Lett.* 1978, **56**, 161. (b) E. Nakazawa, *J. Lumin.* 1979, **18/19**, 272.

[50] P. J. Dean, E. G. Schönherr and R. B. Zetterstrom, *J. Appl. Phys*., 1970, **41**, 3475.
[51] S. J. Gwak, P. A. Kumar and W. B. Im, *J. Phys. Chem. C*, 2014, **118 (5),** 2686.

Table of Content

Fluorescence

Rare earth-free phosphor GaZnON was synthesized by combustion of unimolar mixture of metal oxides and urea, can be used in WLED.

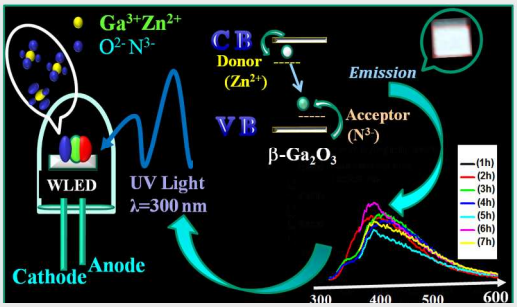

Neelu Chouhan,[a][b]≠ Chun Che Lin,[a]≠ Shu-Fen Hu,[c] and Ru-Shi Liu*[a][d]*

Page No. – Page No.

Rare Earth-Free GaZnON Phosphor Prepared by Combustion for White Light-Emitting Diodes